

Supporting Information

On the Nature of Solvothermally Synthesized Carbon Nanodots

Sergio Ramírez-Barroso,* Alejandra Jacobo-Martín, Iván Navarro-Baena^a, Jaime J. Hernández, Cristina Navio, Isabel Rodríguez and Reinhold Wannemacher*

IMDEA Nanociencia, c/Faraday, 9, 28049 Campo Universitario de Cantoblanco, Spain

^acurrent address: AD Biocomposites, Parque Tecnológico de Paterna, Carrer d'Albert Einstein, 5, 46980 Paterna, Spain

Table of Contents

1. Experimental section.....	1
2. DFT	4
3. Scheme of the process of forming the molecules present in B-CNDs	5
4. UPLC-MS B-CNDs.....	5
5. HR-TEM B-CNDs	6
6. AFM B-CNDs	6
7. DLS B-CNDs	7
8. FTIR B-CNDs	7
9. XPS B-CNDs	8
10. Photophysics of B-CNDs.....	9
11. FCS B-CNDs.....	11
12. Singlet oxygen B-CNDs	12
13. UPLC-MS R-CNDs	13
14. Scheme of the process of forming the molecules present in R-CNDs	14
15. DLS R-CNDs	14
16. FTIR R-CNDs	15
17. Photophysics of R-CNDs	16

1. Experimental section

Synthesis and purification of CNDs

Citric acid (Sigma Aldrich, 99 %), ethylenediamine (Fluka Analytical, 99,5 %), p-phenylenediamine (Sigma Aldrich, 98 %) and absolute ethanol (Merck, 99.5 %) were used to synthesize the carbon dots. Its purification was done with dialysis tubing cellulose (Merck) of different pore size (1, 14 and 25 kDa molecular weight cut-off MWCO) in the dark, as well as under ambient illumination. Purification was also carried out by size exclusion chromatography (SEC) using Sephadex G25-80.

Characterization of CNDs

Ultra-performance liquid chromatography coupled with electrospray ionization quadrupole time-of-flight tandem mass spectrometry (UPLC-ESI-Q-TOF-MS/MS) was carried out using an ACQUITY UPLC system coupled with high resolution mass spectrometer MAXIX II Bruker. Chromatography was performed using a Waters UPLC C18 column (2.1 mm × 5 cm) packed with 1.7 μm octadecyl (C18) bonded silica. The mobile phase contains 0.1 % formic acid (FA) in water (pH 2.8) as eluent A and MeOH or acetonitrile as eluent B for the B-CNDs or R-CNDs respectively. The flow rate was 0.1 mL/min, whose composition by volume was 98 % A and 2 % B. Unless otherwise stated, the optimized source conditions were set as follows: capillary voltage, 3.5 kV; desolvation temperature, 300 °C; and desolvation gas (N₂) flow rate, 8 L/min. The MS range was scanned from 20 Da to 3000 Da and centroided during acquisition using an internal reference (lock spray). Data processing was carried out with Bruker Compass DataAnalysis 4.4 software.

High-resolution transmission electron microscopy (HR-TEM) was carried out using the JEM GRAND ARM300cF with ETA (Expansion Trajectory Aberration Correction) consisting of dodeca-poles (JEOL) on the objective lens and a FEG. The electron accelerating voltage used was 60 kV. Scanning Transmission Electron Microscopy (STEM) was carried out using the JEOL JEM ARM200Cf with CEOS aberration corrector on the field effect emission condenser (cold FEG) lens and HAADF imaging with a JEOL detector and Gatan ABF and HAADF detectors. In this case, the electron acceleration voltage used was 80 kV.

Grazing incidence wide angle X-ray scattering (GIWAXS) measurements was performed at the BL-11 NCD-SWEET beamline of the ALBA synchrotron at Barcelona, Spain. The X-ray patterns were recorded with a WAXS LX255-HS detector from Rayonix (pixel size 80x80 μm²). The norm of the reciprocal space q-vector ($q=4\pi\sin\theta/\lambda$, where θ is the Bragg angle and λ is the wavelength) was calibrated using a chromium oxide (Cr₂O₃) standard. Temperature dependence measurements were performed by using a Linkam heating plate coupled to a precision stage with vertical, horizontal and rotational motions.

Atomic force microscopy (AFM) was carried out on a NT-MDT NTEGRA instrument in dynamic mode. The hydrodynamic size of the CNDs was measured by dynamic light scattering (DLS) from a dilute suspension of the sample in water at pH 7 in a standard cuvette, using a Zetasizer NanoZS device (Malvern Instruments).

Surface-enhanced micro-Raman spectroscopy (SERS) was carried out using an inverted Nikon Eclipse Ti microscope (objective lens 100x/0.8 NA) coupled to a Shamrock SR303i spectrograph equipped with a Peltier-cooled CCD camera (Andor Newton). The home-built set-up allowed excitation of the Raman signals by a helium-neon laser operating at 632.8 nm. The laser was attenuated in order to avoid graphitization of the sample by the excitation. To produce the SERS effect, a commercial gold electrode was used, the surface of which was nano-roughened by cycling in 0.1 M KCl. Absence of the

formation of Au oxides was confirmed by cyclic voltammetry. Samples of the B-CDs, R-CNDs and the dialysate, respectively, were drop-cast on the nano-roughened gold surface and allowed to dry.

Attenuated total internal reflection Fourier-transform infrared spectroscopy (ATR-FTIR) was carried out using a Bruker Alpha spectrometer. XPS (X-ray Photoelectron Spectroscopy) measurements were performed under Ultra High Vacuum conditions (UHV, with a base pressure of 5×10^{-10} mbar), using a monochromatic Al K α line as exciting photon source for core level analysis ($h\nu = 1486.7$ eV). The emitted photoelectrons were collected in a hemispherical energy analyzer (SPHERA-U7, pass energy set to 20 eV for the XPS measurements to have a resolution of 0.6 eV) and to compensate the charge built up on the sample surface the use of a Flood Gun (FG-500, Specs) was employed, with low energy electrons of 3 eV and 40 μ A. Binding energy was corrected using the Si 2p_{3/2} level at 99.3 eV.

UV-Vis absorption spectra were recorded on a UV-Vis spectrophotometer (Varian Cary 50) using 1 cm quartz cuvette (Suprasil). Room-temperature PL and PLE spectra were acquired on a spectrofluorimeter (Horiba FluoroLog 3) equipped with a high-pressure Xenon lamp and a Hamamatsu R928P photomultiplier tube; the PLE and PL spectra were corrected for the characteristics of the lamp source and of the detection system, respectively. The quantum yields of B-CNDs and their dialyzed material were obtained by a relative method using quinine sulphate (QY = 55 % in 0.5 M H₂SO₄), adjusting the optical absorbance to 0.1 at 350 nm and integrating the fluorescence intensity between 370 and 600 nm. Fluorescence quantum yields of the R-CNDs and their dialyzed material were determined by a relative method using rhodamine B (QY = 56 % in ethanol). To obtain reliable results the optical absorbance was adjusted to 0.1 at 510 nm and the fluorescence intensity was integrated between 580 and 610 nm.

PL lifetimes (τ_f) were measuring via time-correlated single photon counting (TCSPC) employing an Acton SP2500 spectrometer equipped with a PMA 06 photomultiplier (PicoQuant) and a HydraHarp-400 TCSPC event timer with 1 ps time resolution. The excitation source was a 405 nm picosecond pulsed diode laser (LDH-D-C-405, PicoQuant) driven by a PDL828 driver (PicoQuant) with FWHM < 70ps. Fluorescence decays were analyzed using PicoQuant Fluofit v4.6.5 data analysis software.

Time-resolved detection of phosphorescence ¹O₂ was performed using a customized Fluotime 200 fluorescence lifetime system (PicoQuant, Germany) described elsewhere. Briefly, for ¹O₂ phosphorescence measurements, an AO-Z-473 solid state AOM Q-switched laser (Changchun New Industries Optoelectronics Technology Co., Changchun, China) working at a 4 kHz repetition rate (<1.5 mW average power) was used for excitation at 473 nm. In order to remove any residual component of its fundamental emission in the NIR region, a 1064-nm rugate notch filter (Edmund Optics, U.K.) and an uncoated SKG-5 filter (CVI Laser Corporation) were placed at the exit port of the laser. The NIR luminescence exiting from the side of the sample was filtered by a long-pass filter of 1000 nm and a narrow bandpass filter at 1270 nm. In this way any scattered laser radiation was removed and the NIR emission from singlet oxygen was isolated. A thermoelectrically cooled Hamamatsu NIR sensitive photomultiplier tube assembly (H9170-45, Hamamatsu, Japan) coupled to a multichannel scaler (Nanoharp 250, PicoQuant) was used for single photon counting detection. The time-dependent ¹O₂ phosphorescence signal $S(t)$ was analyzed using the GraphPad Prism 7 software to fit the data to eq 1, in which τ_T and τ_Δ are the lifetimes of the photosensitizer triplet state and of ¹O₂ respectively, and $S(0)$ is a pre-exponential parameter proportional to Φ_Δ .

$$S_{1270}(t) = S_{1270}(0) \times \frac{\tau_\Delta}{\tau_\Delta - \tau_T} \times \left(e^{-t/\tau_\Delta} - e^{-t/\tau_T} \right) \text{ eq. 1}$$

The Φ_{Δ} values of the different samples were obtained by comparison of the slopes of $S(0)$ vs. absorbed-laser-energy plots obtained at different sample and reference concentrations (eq. 2).

$$\Phi_{\Delta, sample} = \Phi_{\Delta, ref} \times \frac{Slope_{sample}}{Slope_{ref}} \quad eq.2$$

Flavin mononucleotide (Chemodex Ltd. Switzerland) was used as reference ($\Phi_{\Delta} = 0.56 \pm 0.05$).

Fluorescence correlation spectroscopy was performed using an Olympus Ix83 inverted microscope, coupled to a confocal system Olympus FV1200, with 3 confocal detectors (two of them spectral) and one transmitted light, 7 lines of laser, of which 405 and 458 nm were used. The latter is equipped with a motorized stage, an autofocus system (ZDC) and temperature control. The fitting model used was pure diffusion: this assumes that exclusively diffusion contributions are present in the FCS curve (as opposed to contributions from, e.g., triplet states or blinking). The equations used were:

$$G(t) = \sum_{i=0}^{n_{Diff}-1} \frac{\rho[i]}{\left[1 + \frac{t}{\tau_{Diff}[i]}\right] \left[1 + \frac{t}{\tau_{Diff}[i] \kappa^2}\right]^{0.5}}$$

$$N = \left[\sum_{i=0}^{n_{Diff}-1} \rho[i] \right]^{-1} \quad eq. 4$$

$$C = \frac{N}{V_{Eff} N_A} \quad eq. 5$$

$$w_0 = \left[\frac{V_{Eff}}{\kappa} \right]^{\frac{1}{3}} - 0.5 \quad eq. 6$$

$$z_0 = \kappa w_0 \quad eq. 7$$

$$D[k] = \frac{w_0^2}{4 \tau_{Diff}[k]} \quad eq. 8$$

$$R_H = \frac{4 k_B T \tau_{Diff}}{6 \pi \eta w_0^2} \quad eq. 9$$

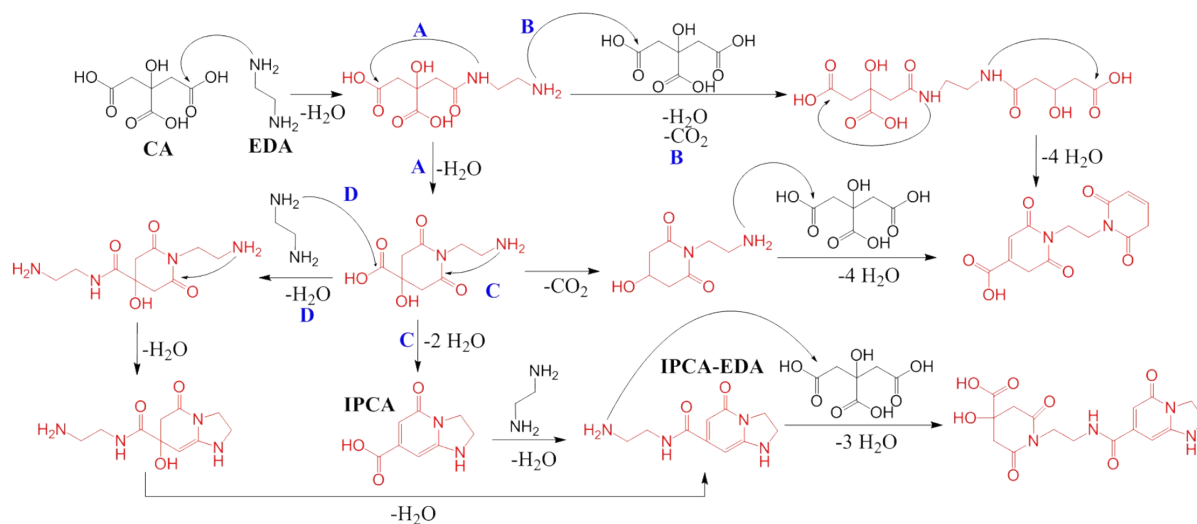
2. DFT

DFT calculations were performed using the Firefly QC package [1], which is partially based on the GAMESS (US) [2] source code, based on the B3LYP [3] functional

[1] Alex A. Granovsky, Firefly version 8.0.0, <http://classic.chem.msu.su/gran/firefly/index.html>

[2] M.W.Schmidt, K.K.Baldrige, J.A.Boatz, S.T.Elbert, M.S.Gordon, J.H.Jensen, S.Koseki, N.Matsunaga, K.A.Nguyen, S.Su, T.L.Windus, M.Dupuis, J.A.Montgomery *J. Comput. Chem.* 1993, **14**, 1347-1363.

3. Scheme of the process of forming the molecules present in B-CNDs



Scheme 1. Process of forming the molecules present in B-CNDs from citric acid (CA) and ethylene diamine (EDA). Molecules in red are those identified by UPLC-MS.

4. UPLC-MS B-CNDs

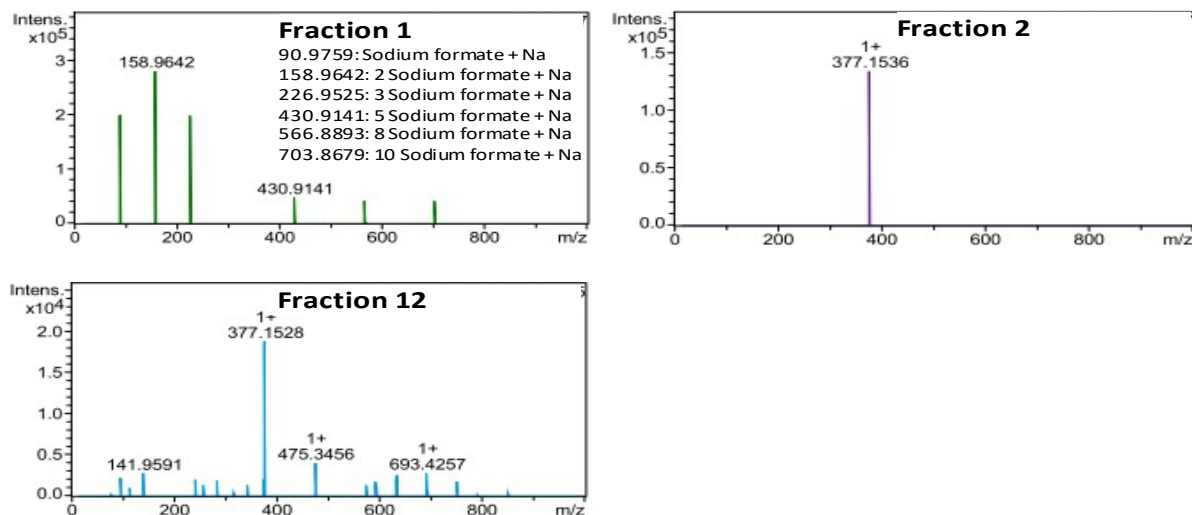


Fig. S1. MS spectra of the fractions observed in B-CNDs coming from the blank.

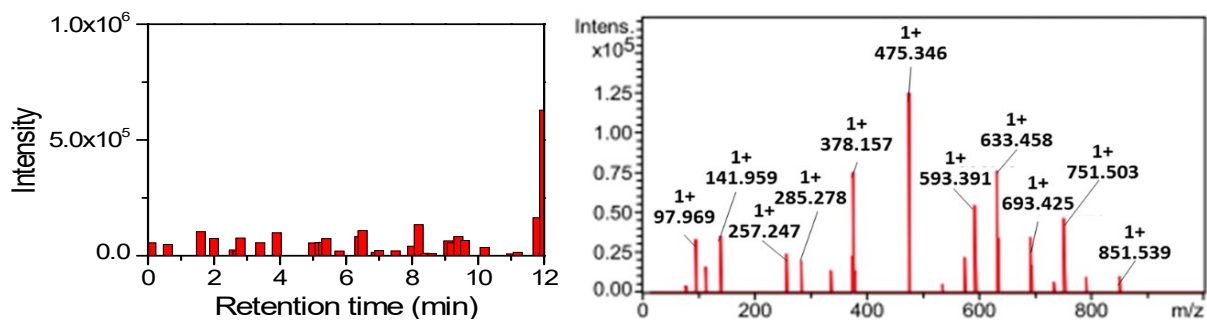


Fig. S2. Gradient elution of the blank sample. The chromatograms are monitored with ESI-Q-TOF MS/MS detection and representative MS spectra.

5. HR-TEM B-CNDs

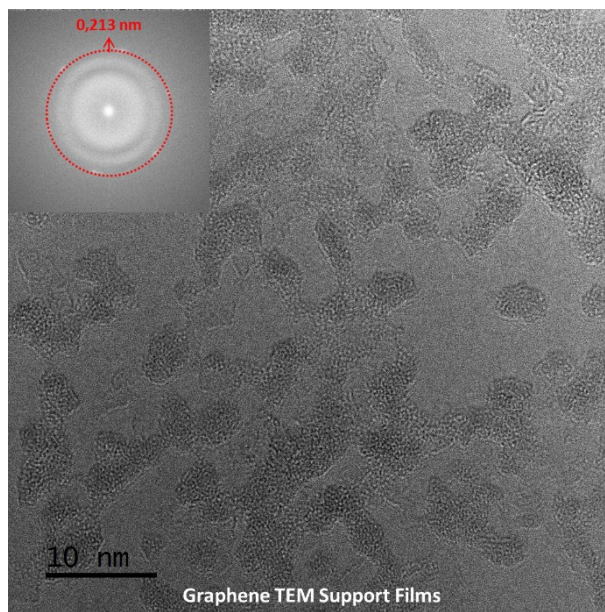


Fig. S3. Representative HR-TEM images and fast Fourier transform (FFT) diffraction patterns of graphene TEM Support films.

6. AFM B-CNDs

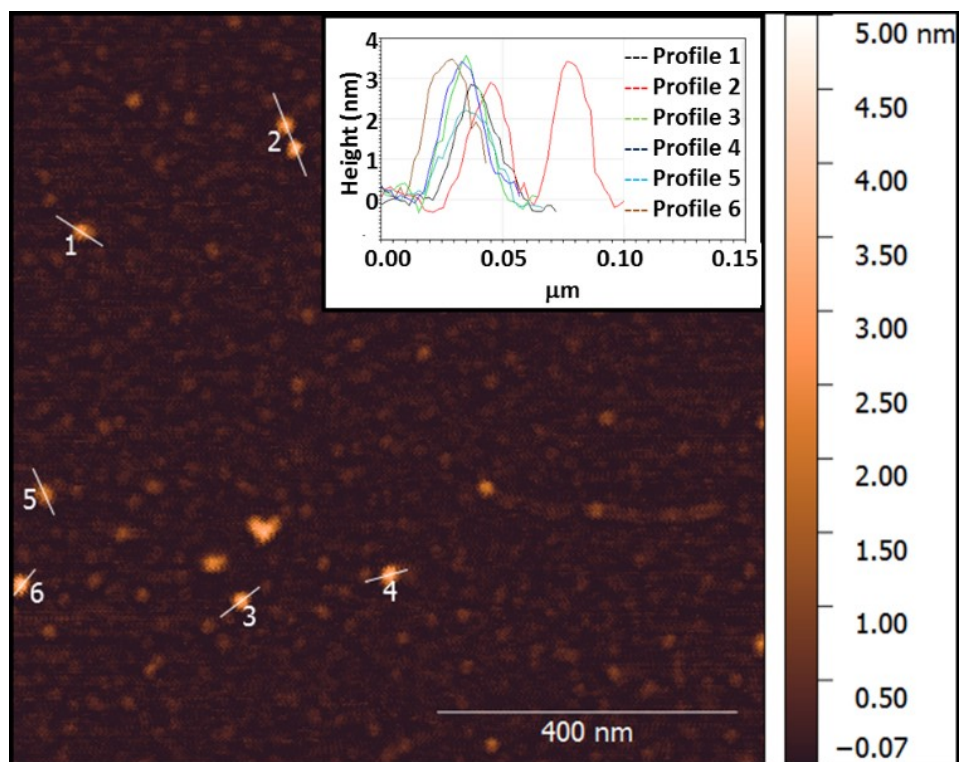


Fig. S4. Representative AFM images and height profiles of B-CNDs.

7. DLS B-CNDs

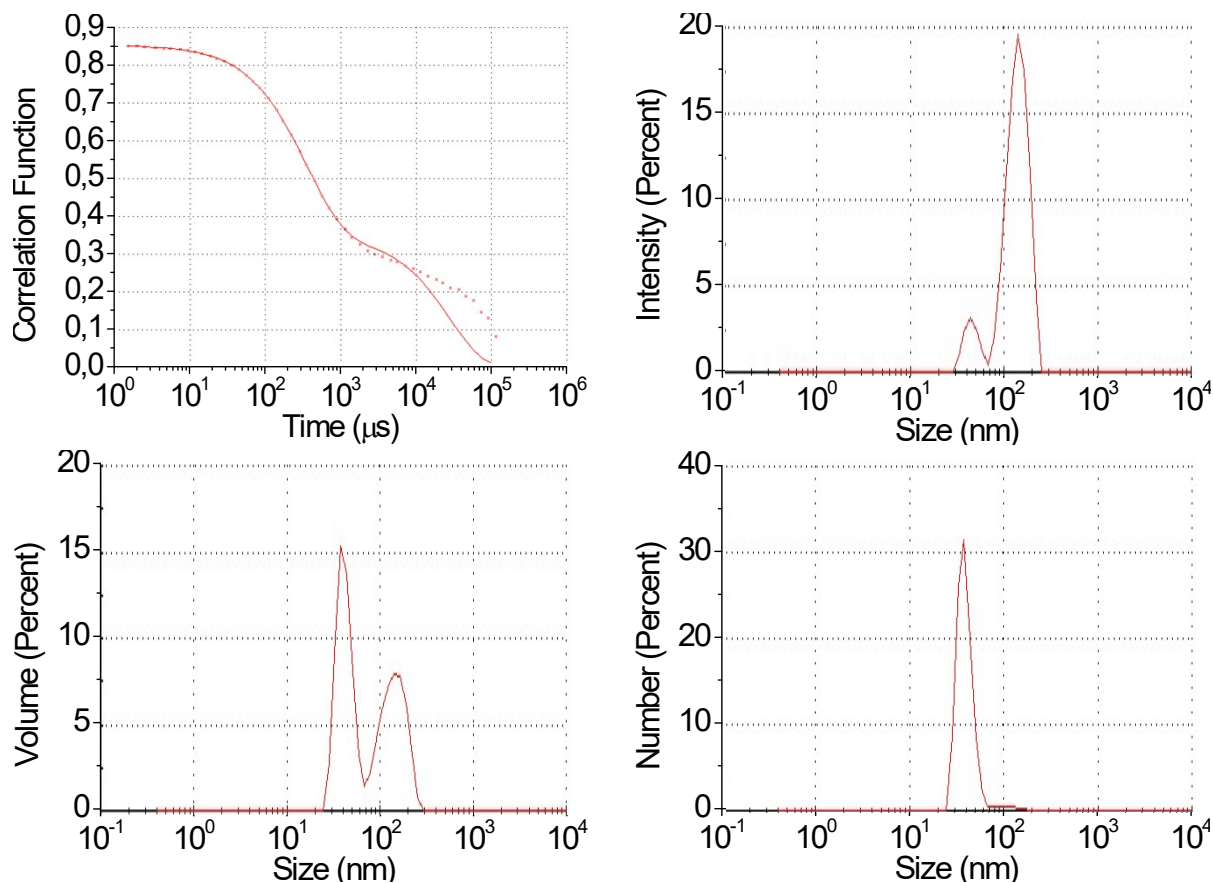


Fig. S5. Correlogram and size distribution analysis by DLS by intensity, volume or number of B-CNDs in water at pH 7.4.

8. FTIR B-CNDs

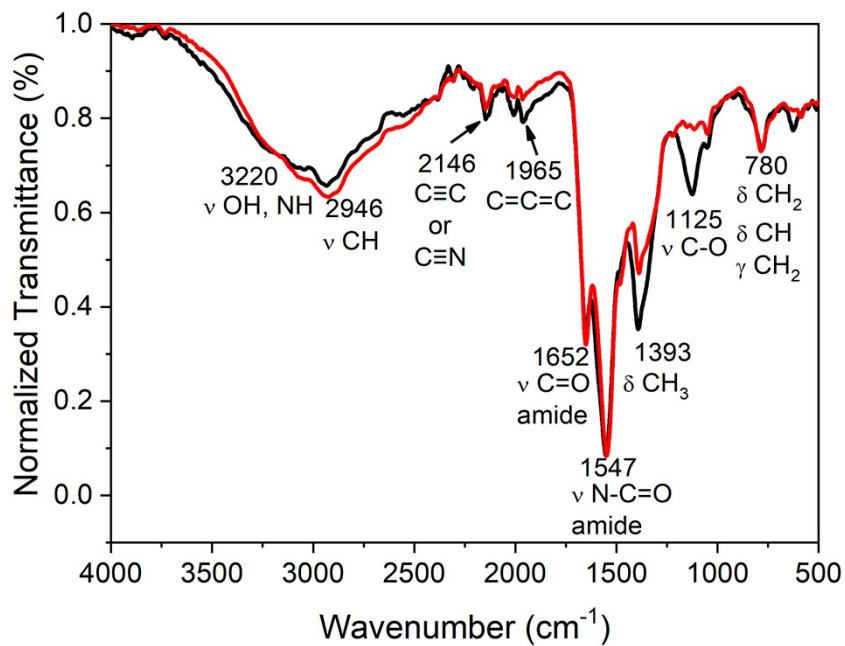


Fig. S6. Attenuated total reflection Fourier-transform infrared (ATR-FTIR) spectra of dialyzed material and B-CNDs. Distinct vibration bands corresponding to B-CNDs surface groups are indicated.

9. XPS B-CNDs

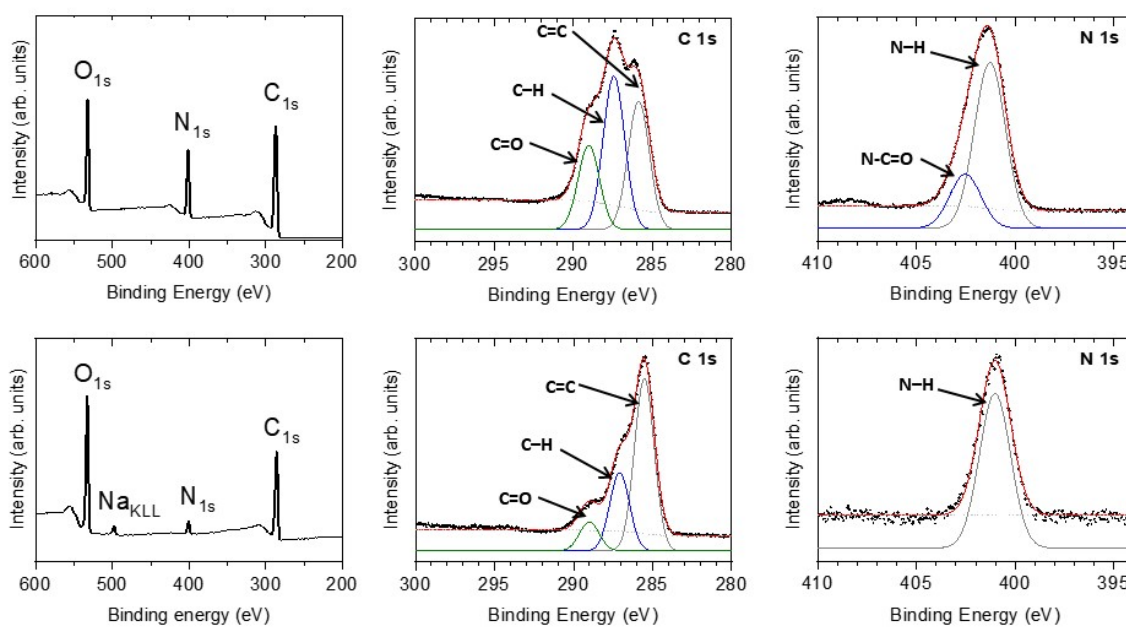


Fig S7. XPS spectra of dialyzed material (upper row of figures) and B-CNDs (lower row).

10. Photophysics of B-CNDs

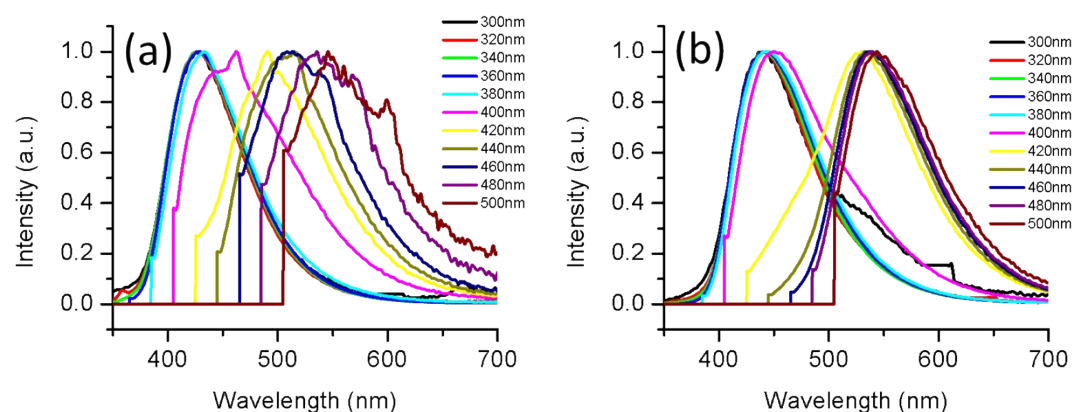


Fig S8. Normalized PL spectra, as obtained from the emission excitation maps of Fig. 5. (a) of the B-CNDs and (b) the dialysate after 14 days under ambient illumination. Small peaks in the spectra correspond to Raman signals of the water.

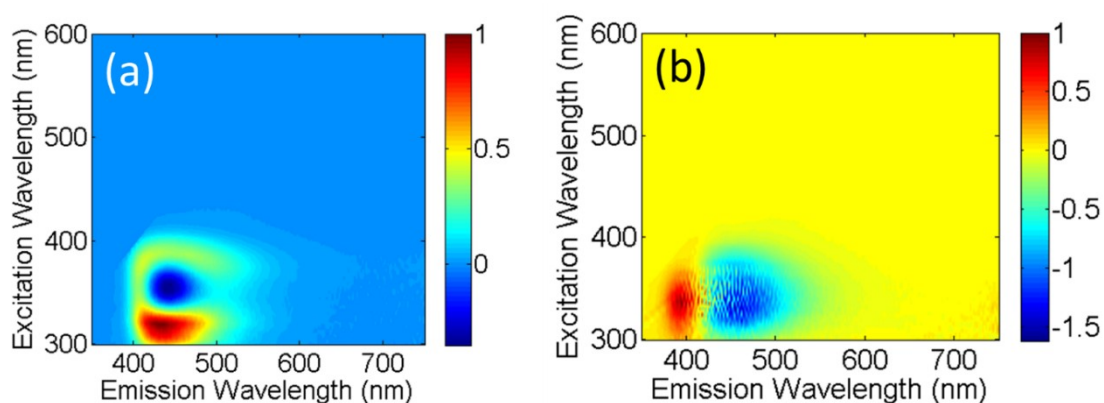


Fig S9. Differential excitation-emission map of the dialysate Figure S8a) and the retentate (B-CNDs, Figure S8b) after 14 days in the dark and immediately after collection / dialysis in the dark, respectively.

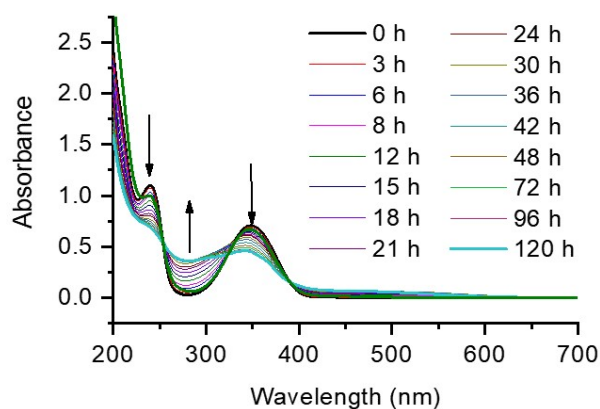


Fig. S10. Evolution of the UV-Vis absorption of the dialyzed material when exposed to ambient light for 120 hours.

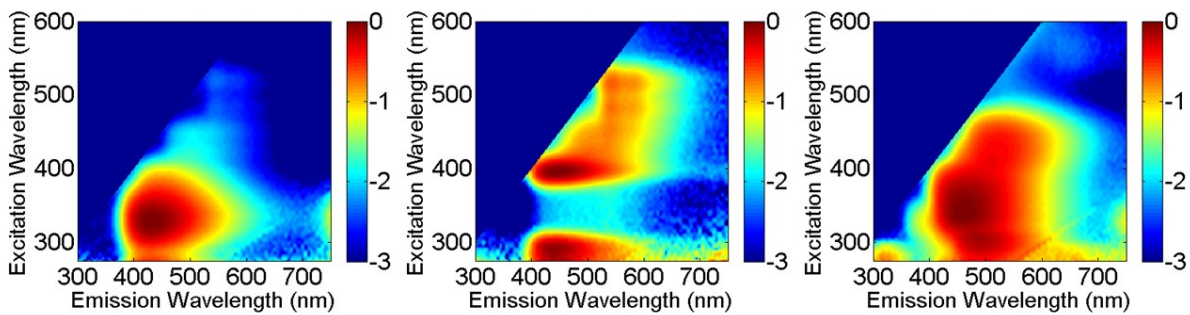


Fig. S11. Excitation-emission maps of the most representative fractions (Fractions 1, 5 and 14, respectively) obtained by size exclusion chromatography.

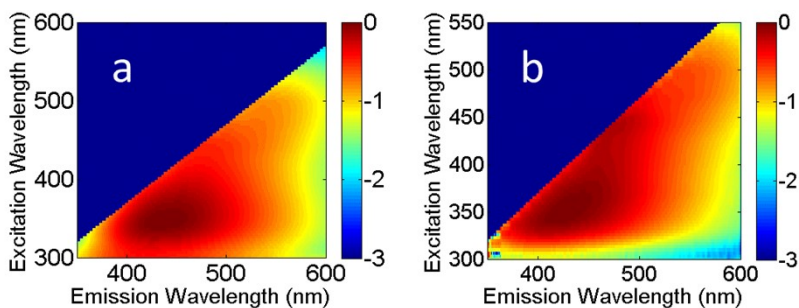


Fig. S12. Excitation-emission maps of the B-CNDs incorporated in water-soluble polymers such as (a) polyvinylpyrrolidone (PVP) and (b) polyvinyl alcohol (PVA)

11. FCS B-CNDs

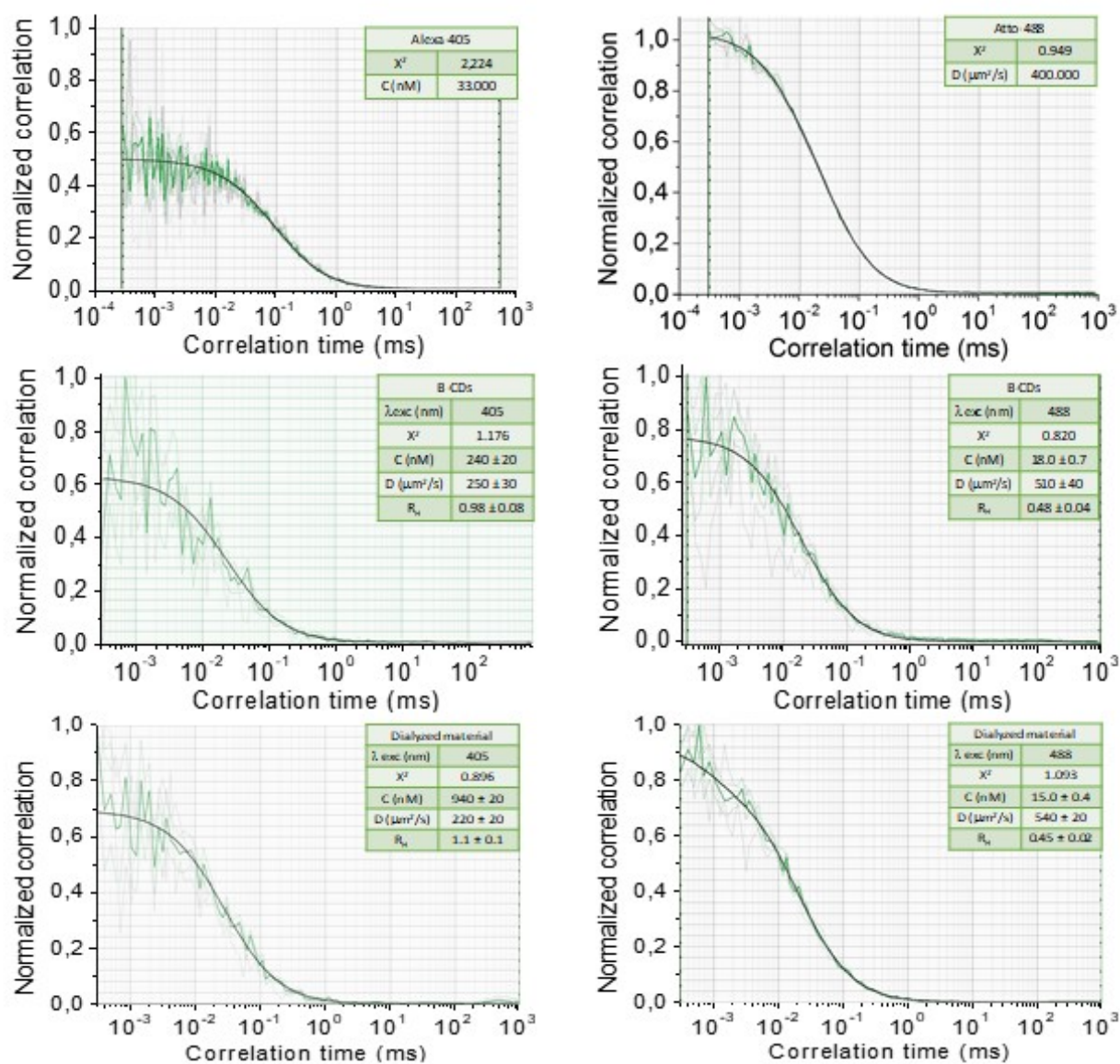


Fig. S13. Normalized FCS curves for the standards used (up), B-CNDs (middle) and the dialysate material (down), under 405 and 488 nm excitation (left and right, respectively).

12. Singlet oxygen B-CNDs

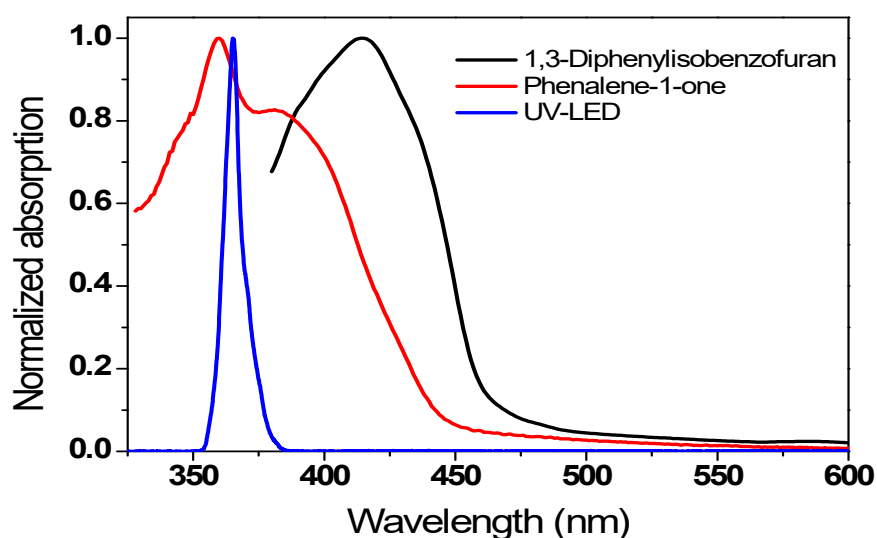


Fig. S14. UV-Vis absorption spectra of phenalene-1-one as singlet oxygen photosensitizer, 1,3-diphenylisobenzofuran as singlet oxygen trap and the emission of a UV LED ($\lambda_c = 365$ nm) used for illumination.

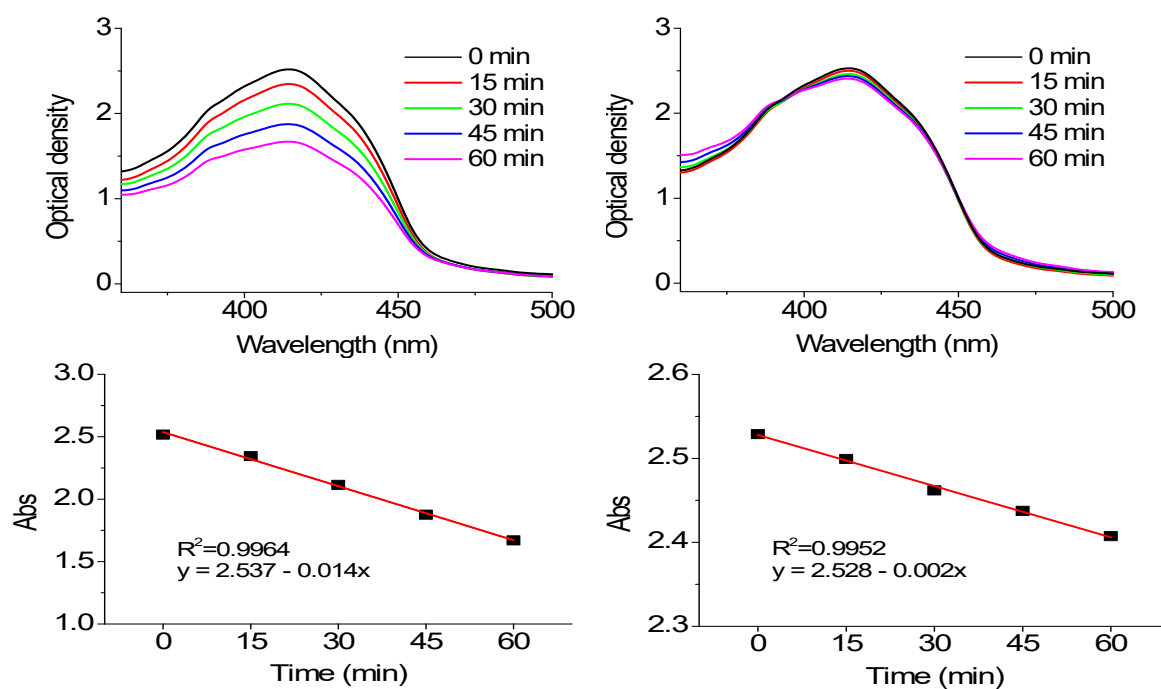


Fig. S15. Photodegradation of 1,3-Diphenylisobenzofuran in the presence of phenalene-1-one only (left) or in the presence of phenalene-1-one and dialyzed material (right) under UV-LED.

13. UPLC-MS R-CNDs

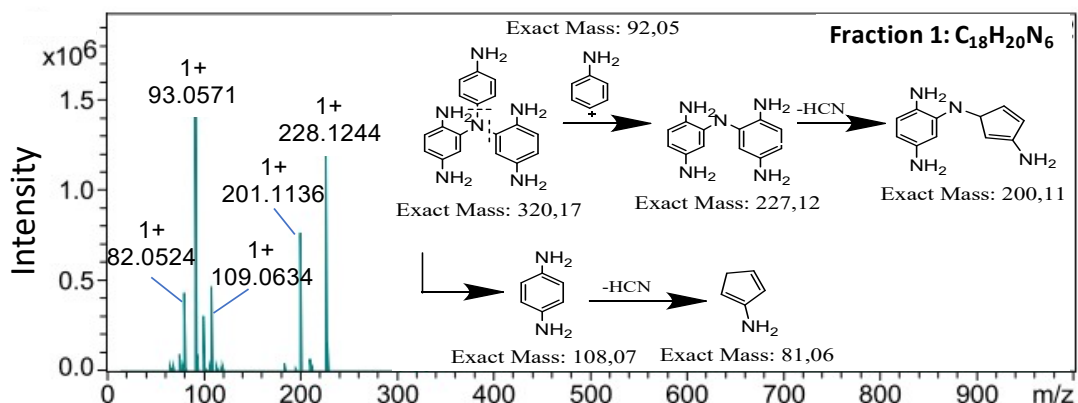


Fig. S16. MS/MS spectrum of fraction 1 of R-CNDs to elucidate the structural isomer present.

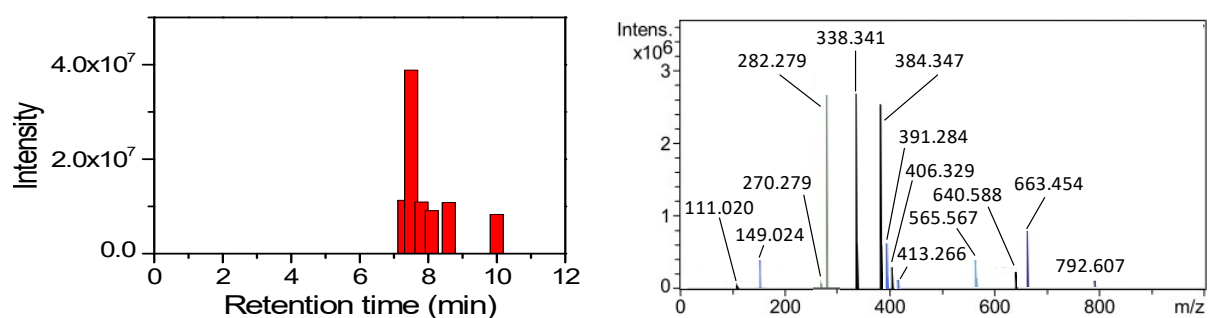
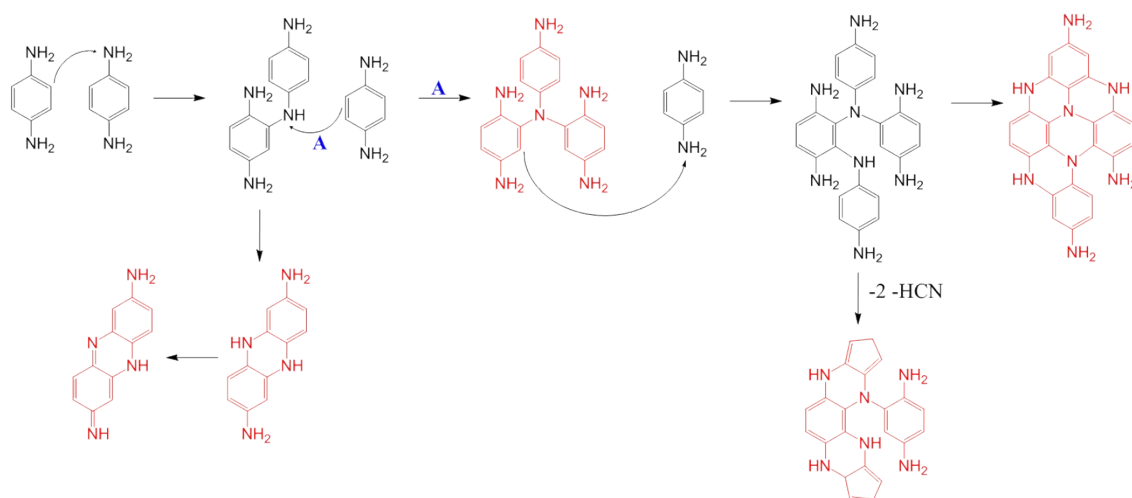


Fig. S17. Gradient elution of the blank sample. The chromatograms are monitored with ESI-Q-TOF MS/MS detection and representative MS spectra.

14. Scheme of the process of forming the molecules present in R-CNDs



Scheme 2. Process of forming the molecules present in R-CNDs from p-Phenylenediamine. Molecules in red are those identified by UPLC-MS.

15. DLS R-CNDs

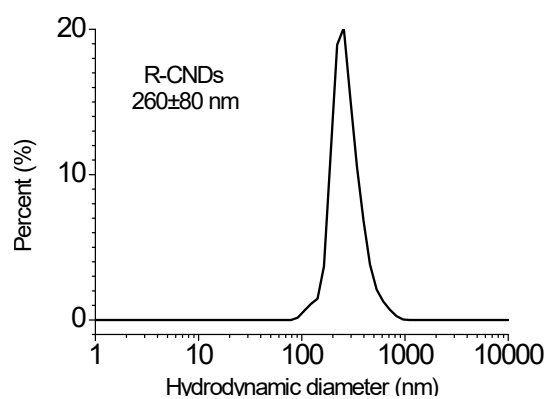


Fig. S18. Correlogram and size distribution analysis by DLS of R-CNDs in water at pH 7.4.

16. FTIR R-CNDs

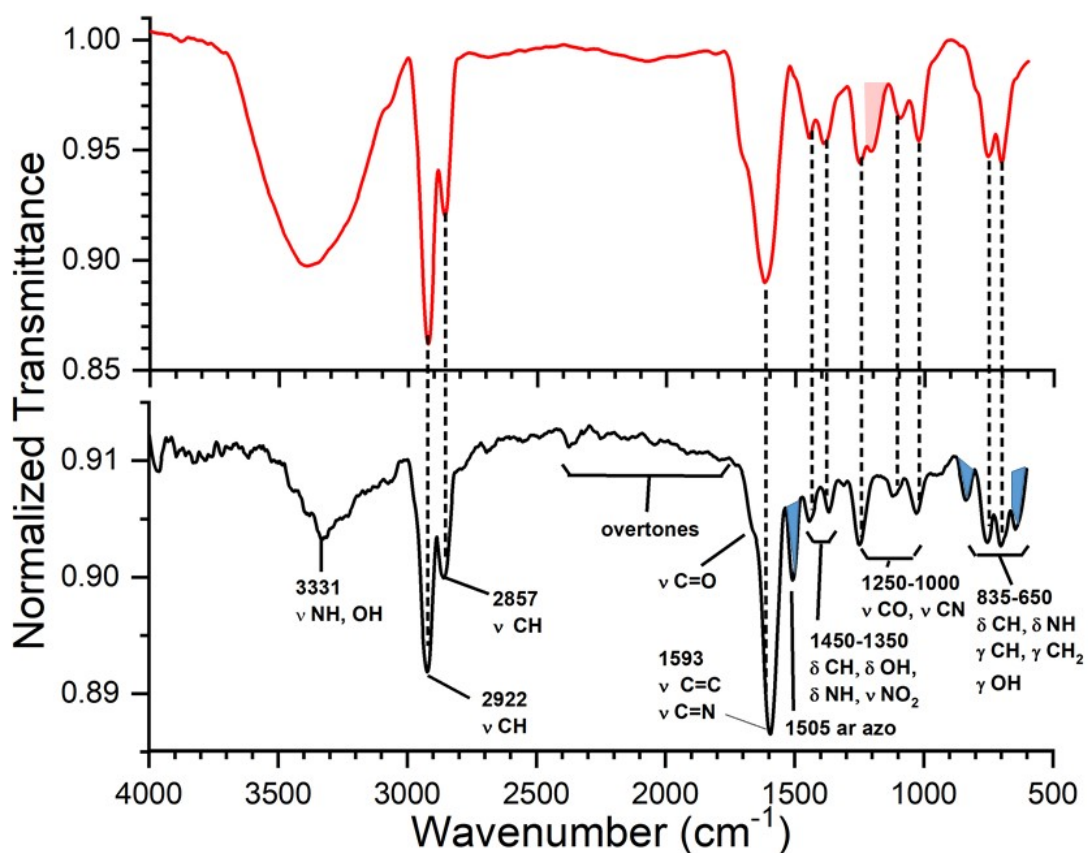


Fig. S19. Normalized attenuated total reflection Fourier-transform infrared (ATR-FTIR) spectra of dialysate (red, top graph) and R-CNDs (black, bottom graph). Vibration bands corresponding to R-CNDs surface groups are indicated as blue-shaded areas. A single band occurring in the dialysate, but not in the R-CNDs, is marked in red.

17. Photophysics of R-CNDs

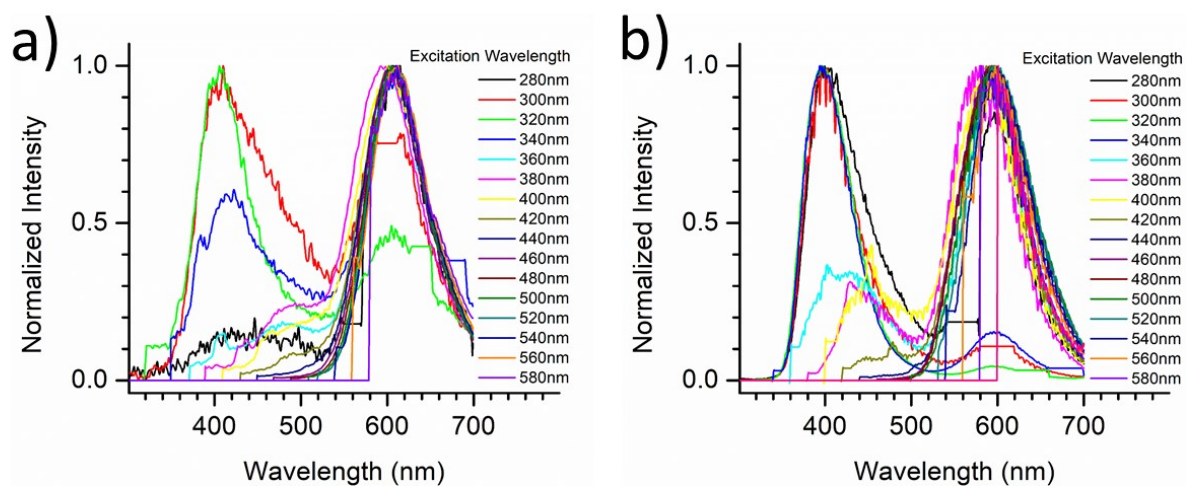


Fig. S20. Selected normalized PL spectra, corresponding to the maps of Figure 10, of (a) R-CNDs and (b) the dialyzed material as a function of the excitation wavelength. Sharp peaks correspond to Raman signals from the water. Plateaus are caused by the automatic protection electronics of the photomultiplier in order to avoid saturation due to the second order of the excitation.